Mechanism of enhanced energy storage density in AgNbO3-based lead-free antiferroelectrics

LU, Zhilun, BAO, Weichao, WANG, Ge, SUN, Shi-Kuan, LI, Linhao, LI, Jinglei, YANG, Huijing, JI, Hongfen, FETEIRA, Antonio <http://orcid.org/0000-0001-8151-7009>, LI, Dejun, XU, Fangfang, KLEPPE, Annette K, WANG, Dawei, LIU, Shi-Yu and REANEY, Ian M

Supplementary information

Mechanism of enhanced energy storage density in $AgNbO_3$-based lead-free antiferroelectrics

Zhilun Lu[a,b,1], Weichao Bao[c,1], Ge Wang[a,1], Shi-Kuan Sun[a,1], Linhao Li[a], Jinglei Li[d], Huijing Yang[a,e], Hongfen Ji[a,f], Antonio Feteira[g], Dejun Li[h], Fangfang Xu[c], Annette K. Kleppe[i], Dawei Wang[a,*], Shi-Yu Liu[h,*], Ian M. Reaney[a,*]

[a]Department of Materials Science and Engineering, University of Sheffield, Sheffield, S1 3JD, UK.

[b]The Henry Royce Institute, Sir Robert Hadfield Building, Sheffield, S1 3JD, UK.

[c]State Key Laboratory of High Performance Ceramics and Superfine Microstructure, Shanghai Institute of Ceramics, Shanghai, 200050, China.

[d]Electronic Materials Research Laboratory, Key Laboratory of the Ministry of Education and International Center for Dielectric Research, Xi'an Jiaotong University, Xi'an 710049, Shaanxi, China.

[e]Department of Physics, Tangshan Normal University, Tangshan 063000, China.

[f]Laboratory of Thin Film Techniques and Optical Test, Xi'an Technological University, Xi'an 710032, China.

[g]Materials and Engineering Research Institute, Sheffield Hallam University, Sheffield, S1 1WB, UK.

[h]College of Physics and Materials Science, Tianjin Normal University, Tianjin 300387, China.

[i]Diamond Light Source Ltd, Harwell Science and Innovation Campus, Didcot, OX11 0DE, UK.

*Corresponding authors. E-mail address:

dawei.wang@sheffield.ac.uk, shiyuliu@mail.tjnu.edu.cn, i.m.reaney@sheffield.ac.uk.

#Author Contributions: Z. Lu, W. Bao, G. Wang and S. Sun contributed equally to this work.

Key words: *Energy storage capacitors; Antiferroelectrics; In-situ synchrotron X-ray diffraction; Silver niobate*

Table S1 The reported sequence of phase transitions in $AgNbO_3$.

Phases	Polarizability	Space groups	Transition temperatures (°C)
M1	ferroelectric	*Pbcm/Pmc2₁*	~70
M2	disordered AFE	*Pbcm*	~270
M3	disordered AFE	*Pbcm*	~350
O1	paraelectric	*Cmcm*	~361
O2	paraelectric	*Cmcm*	~387
T	paraelectric	*P4/mbm*	~580
C	paraelectric	*Pm3m*	/

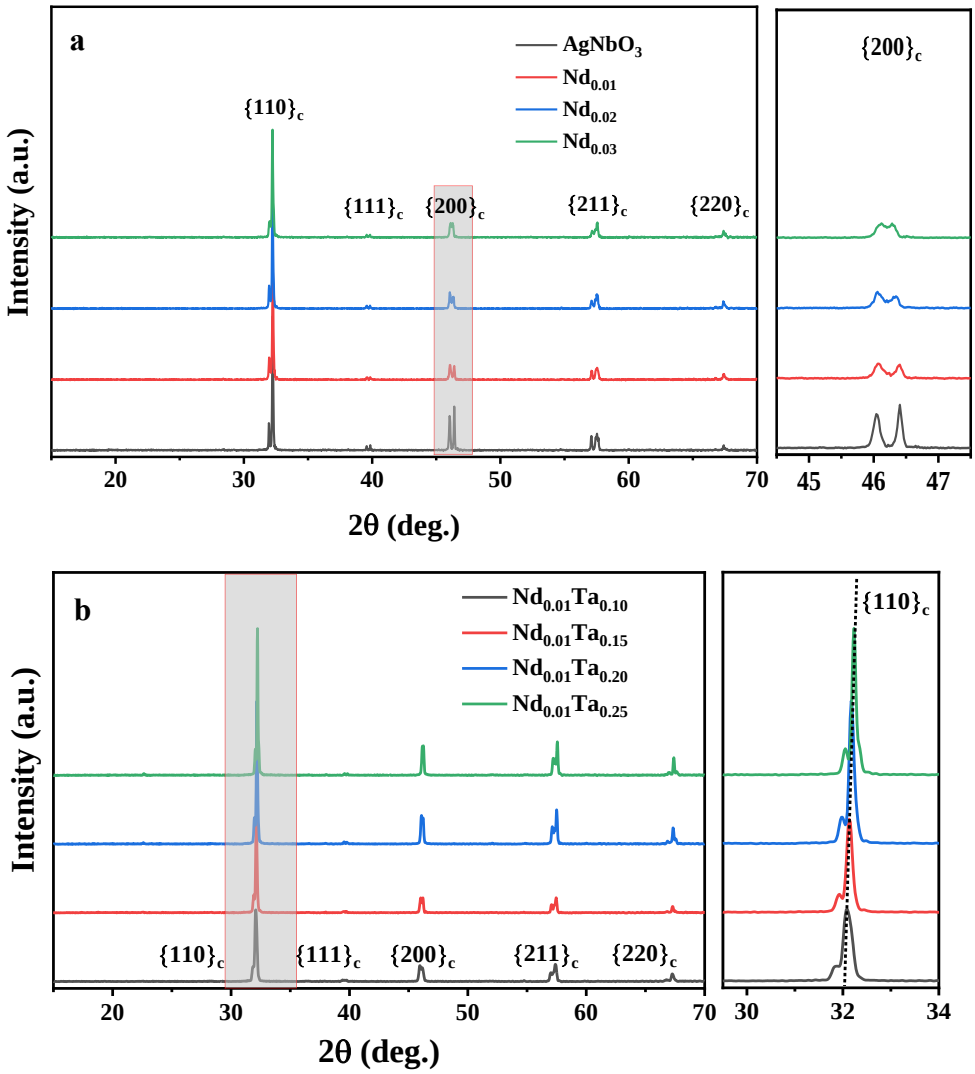

Fig. S1 XRD of all ceramics measured at room temperature.

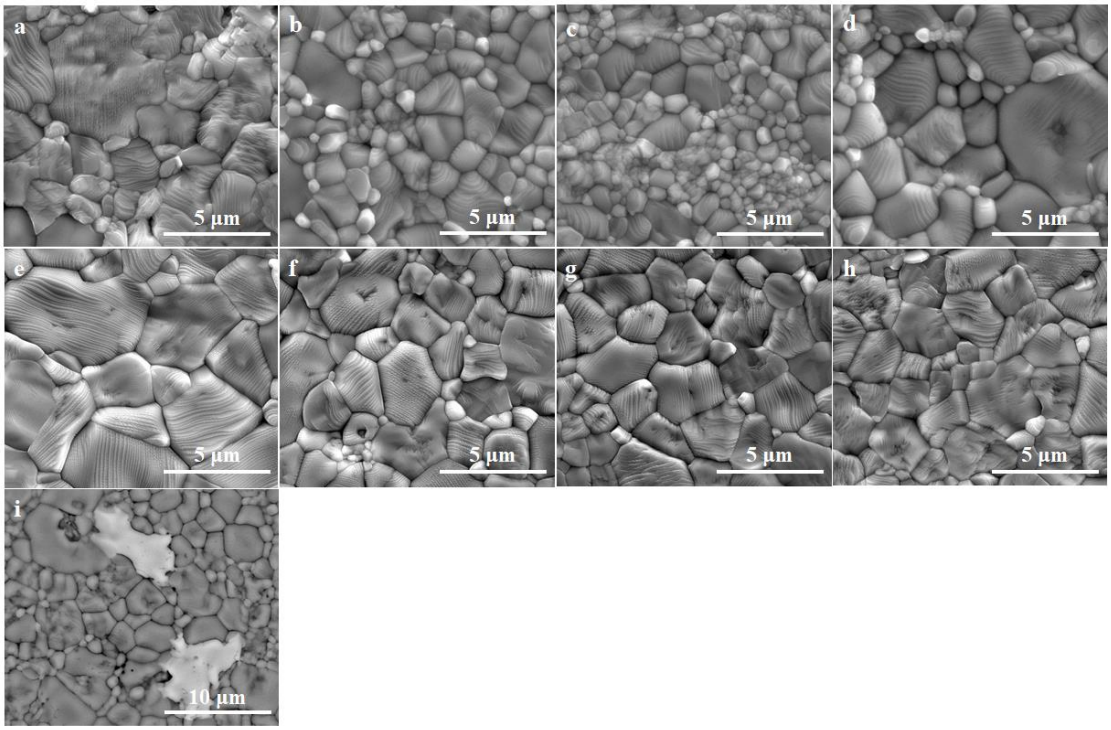

Fig. S2 Secondary electron (SE) images of polished thermal etched samples of a) $AgNbO_3$; b) $Nd_{0.01}$; c) $Nd_{0.02}$; d) $Nd_{0.03}$; e) $Nd_{0.01}Ta_{0.10}$; f) $Nd_{0.01}Ta_{0.15}$; g) $Nd_{0.01}Ta_{0.20}$; h) $Nd_{0.01}Ta_{0.25}$ and i) backscattered electron (BSE) image of a polished thermally etched sample of $Nd_{0.03}$.

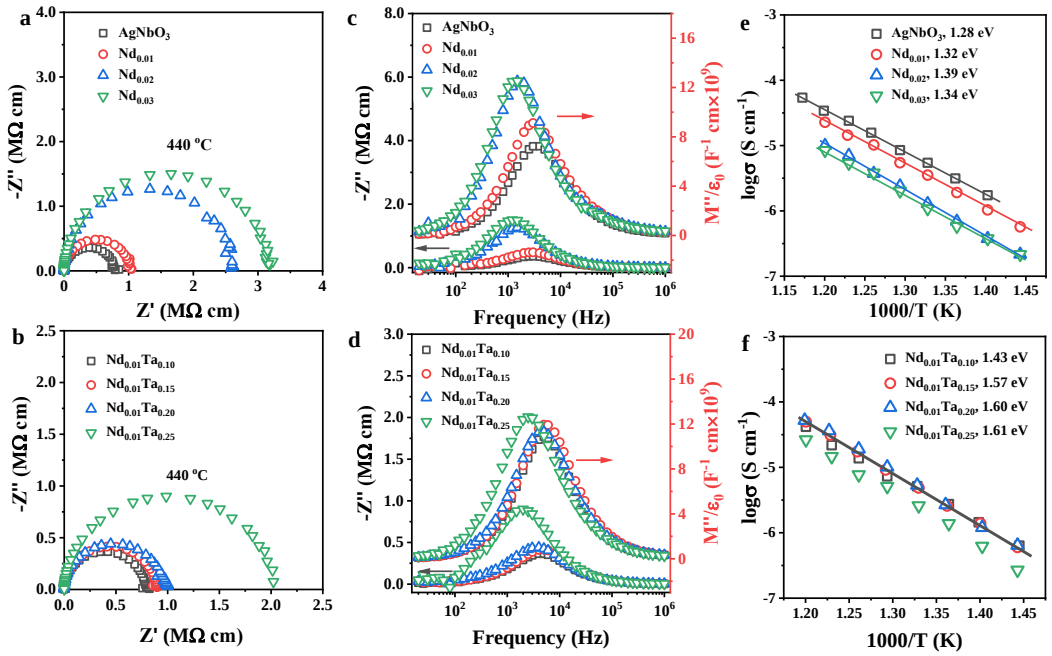

Fig. S3 Impedance spectroscopy data (a-d) and the Arrhenius plots (e, f) of $Ag_{1-3x}Nd_xNbO_3$ and $Ag_{0.97}Nd_{0.01}Ta_yNb_{1-y}O_3$ ceramics.

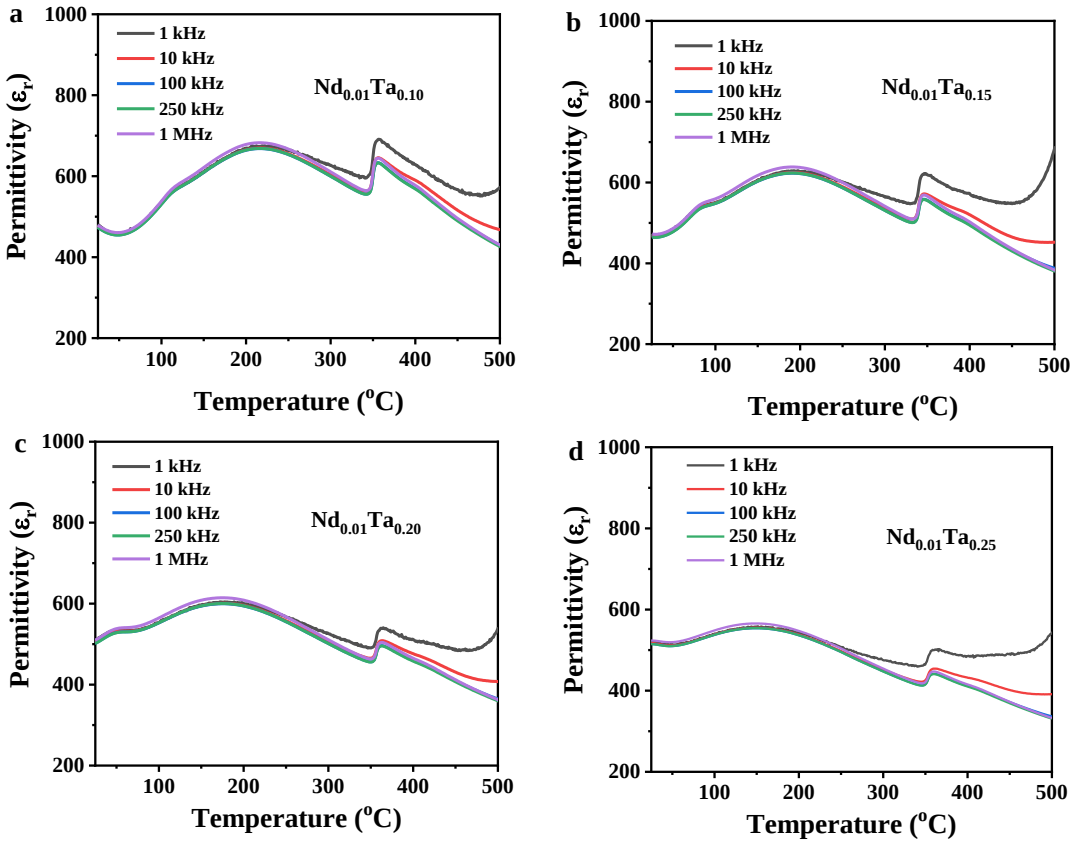

Fig. S4 The frequency dependence permittivity (ε_r *vs* T) and loss ($tan\delta$ *vs* T) for the $Ag_{0.97}Nd_{0.01}Ta_yNb_{1-y}O_3$ ceramics.

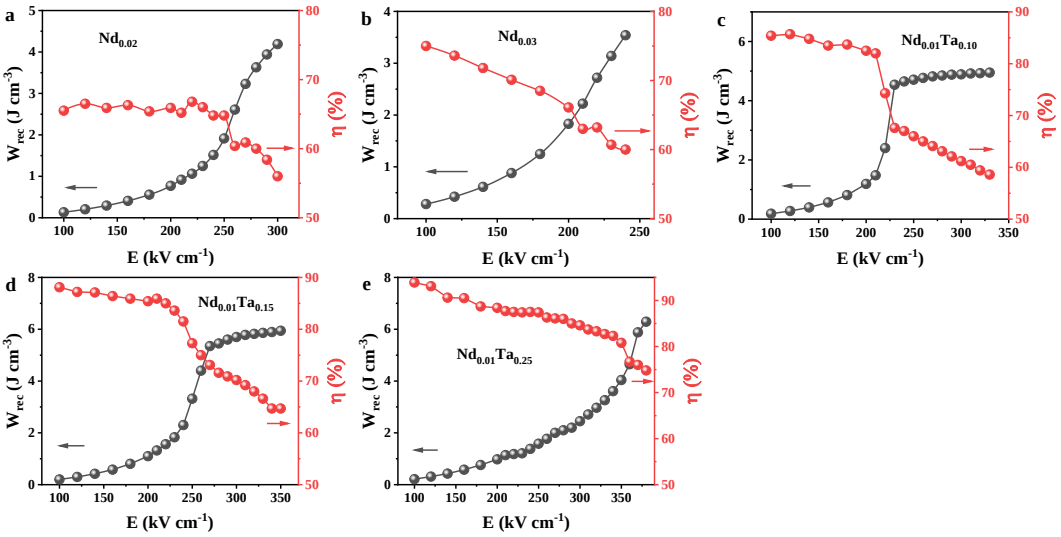

Fig. S5 W_{rec} and η of a) $Nd_{0.02}$; b) $Nd_{0.03}$; c) $Nd_{0.01}Ta_{0.10}$; d) $Nd_{0.01}Ta_{0.15}$ and e) $Nd_{0.01}Ta_{0.25}$ under their respective electric fields.

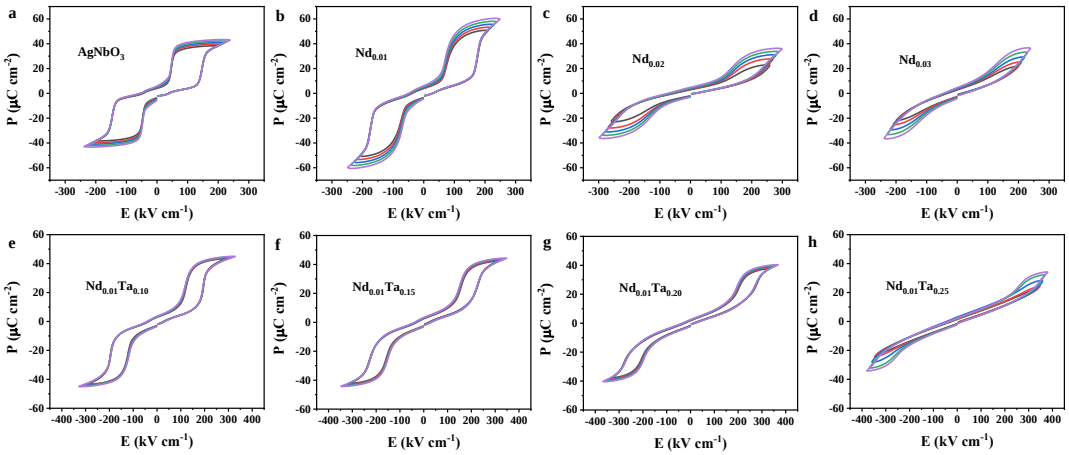

Fig. S6 P-E loops of a) $AgNbO_3$; b) $Nd_{0.01}$; c) $Nd_{0.02}$; d) $Nd_{0.03}$; e) $Nd_{0.01}Ta_{0.10}$; f) $Nd_{0.01}Ta_{0.15}$; g) $Nd_{0.01}Ta_{0.20}$ and h) $Nd_{0.01}Ta_{0.25}$ ceramics under their respective electric fields.

Table S2 Refinement parameters of $Ag_{0.97}Nd_{0.01}Ta_{0.25}Nb_{0.75}O_3$ ceramic at zero field and 380 kV cm^{-1}.

Electric field (kV cm^{-1})	0	380		
Space group	*Pbcm*	*Pmc2₁*	*Pbcm*	*Pb2₁m*
Unit cell volume (Å^3)	484.62(4)	484.81(4)	484.92(4)	484.65(4)
Calculated density (g/cm^3)	7.4276(7)	7.3706(7)	7.3689(7)	7.3731(7)
a (Å)	5.5359(3)	15.6856(9)	5.5824(3)	5.5814(3)
b (Å)	5.5816(3)	5.5359(3)	5.5371(5)	5.5358(3)
c (Å)	15.6839(8)	5.5819(3)	15.6881(6)	15.6856(8)
GoF	1.07	1.02	1.10	1.08
Rexp	9.22	9.52	9.31	9.34
Rwp	9.89	9.71	10.24	10.08

First-principles calculations

The first-principles calculations were performed on the basis of DFT, the pseudopotential method, and plane-wave basis sets [1-3]. The results were obtained by using a Cambridge serial total energy package (CASTEP) [4]. The exchange-correlation effects were treated using the local density approximation (LDA) [5]. For modeling of $Ag_{1-3x}Nd_xTa_yNb_{1-y}O_3$ solid solutions, the virtual crystal approximation (VCA) was adopted which preserves the same crystalline unit cells as $AgNbO_3$ and replacing the Ag (Nb) with the virtual Nd (Ta) atom [6]. The crystal structure of orthorhombic Ag_{1-}

$_{3x}Nd_xTa_yNb_{1-y}O_3$ with a space group of *Pbcm* is shown in Figure 1. A plane-wave cutoff energy of 800 eV was employed in the calculations, which assured a total energy convergence of 10^{-6} eV/atom. For bulk calculations in which primitive unit cells were employed, the Brillouin zone sampling was set with the 9 ×9 ×3 Monkhorst-Pack k-points meshes. All primitive unit cells were relaxed until the force on each atom was smaller than 0.01 eV/Å.

LGD phenomenology theory

According to Kittel's theory [7], an AFE crystal is divided into two neighboring antiparallel dipoles with spontaneous polarizations P_1 and P_2. The total Gibbs free energy g of the AFE system can be written as:

$$G = G_0 + a(P_1^2+P_2^2) + bP_1P_2 + c(P_1^4 + P_2^4) + d(P_1^6 + P_2^6) – (P_1 + P_2)E \quad (1)$$

where a, b, c, and d are the Landau coefficients, and E is the applied electric field, respectively. By calculating the thermodynamics conditions numerically ($\partial G/\partial P_1 = \partial G/\partial P_2 = 0$), the equilibrium relations of P_1 and P_2 can be obtained:

$$2aP_1 + 4cP_1^3 + 6dP_1^5 + bP_2 – E = 0 \quad (2)$$

$$2aP_2 + 4cP_2^3 + 6dP_2^5 + bP_1 – E = 0 \quad (3)$$

Here, we introduce the induced a spontaneous polarization order parameter (P_F) and the AFE structural order parameter (P_A):

$$P_F = (P_1 + P_2)/2, P_A = (P_1 – P_2)/2. \quad (4)$$

Recently, Tolédano et al. proposed a modified LGD phenomenological theory to explain the AFE phase transitions by introducing a coupling term as $\lambda P_A^2 P_F^2$ [8]. High-order items containing the polarization order parameter are neglected and the free energy of the system is:

$$G = G_0(T) + \alpha P_A^2 + \beta P_A^4 + \gamma P_A^6 + \lambda P_A^2 P_F^2 – P_F E, \quad (5)$$

where $G_0(T)$ is the free energy of the paraelectric (PE) phase, α, β, γ, and λ are the constants. E is applied electric field. $\alpha = \alpha_0(T-T_C)$, T_C is the Curie temperature and α_0 a positive constant.

DFT + LGD theory

Table S3 shows the DFT calculated lattice constant (a, b, and c), volume (V) of pure $AgNbO_3$, Nd-doped, and Nd/Ta co-doped $AgNbO_3$ systems with *Pbcm* space group, as well as the total energy

difference between antiferroelectric (AFE) and paraelectric (PE) phases ($\Delta E = E_{AFE} - E_{PE}$) for pure $AgNbO_3$, Nd-doped, and Nd/Ta co-doped $AgNbO_3$. From Table S3, the calculated *V* of Nd-doped $AgNbO_3$ AFEs slightly decreases with the doping of Nd, while the lattice constants and *V* of Nd/Ta co-doped $AgNbO_3$ AFEs increase with the co-substitution of Nd and Ta. ΔE of Nd-doped and Nb/Ta co-doped $AgNbO_3$ decreases with respect to $AgNbO_3$, indicating that the co-doped AFE phase is further stabilized.

Table S3 The DFT calculated lattice constant (a, b, and c), volume (V) of pure $AgNbO_3$ and Nd-doped $AgNbO_3$ (i.e. $Ag_{0.97}Nd_{0.01}NbO_3$) and Nd/Ta co-doped $AgNbO_3$ (i.e. $Ag_{0.97}Nd_{0.01}Ta_{0.2}Nb_{0.8}O_3$) antiferroelectric (AFE) systems with *Pbcm* space group. And total energy difference between antiferroelectric (AFE) and paraelectric (PE) phases ($\Delta E = E_{AFE} - E_{PE}$) for pure $AgNbO_3$, Nd-doped $AgNbO_3$, and Nd/Ta co-doped $AgNbO_3$. For simplicity, the vacancy in the Nd and Ta doped $AgNbO_3$ system was omitted in the DFT calculations. In addition, it should be noticed that $\Delta E = E_{AFE} - E_{PE} = \Delta G = G_{AFE} - G_{PE}$, when the external electric field is zero.

Parameters	$AgNbO_3$	Nd-doped $AgNbO_3$	Nd/Ta co-doped $AgNbO_3$
a (Å)	5.531	5.532	5.561
b (Å)	5.657	5.651	5.699
c (Å)	15.878	15.888	15.988
V ($Å^3$)	496.849	496.726	506.700
ΔE (eV)	-4.765	-4.886	-4.910

Based on LGD theory, the free energy difference (ΔG) for the system:

$$\Delta G = G - G_0(T) = \alpha P_A^2 + \beta P_A^4 + \gamma P_A^6 + \lambda P_A^2 P_F^2 - P_F E \quad (6)$$

$$\alpha = \alpha_0 (T\text{-}T_C), \quad (7)$$

$$P_A = P_1 - P_2 \quad (8)$$

$$P_F = P_1 + P_2 \quad (9)$$

where *G* is free energy of the system, $G_0(T)$ is the free energy of PE phase, α, β, γ, and λ are constants. *E* is the applied electric field. T_C is the Curie temperature and α_0 is a positive constant. P_1 and P_2 are the two neighboring spontaneous polarizations in the lattice. Fig. S7 shows the schematic contour maps of ΔG for $AgNbO_3$, Nd-doped $AgNbO_3$, and Nd/Ta co-doped systems without and with *E*. $G_{AFE} = E_{tot}$ (AFE) and $G_{PE} = E_{tot}$ (PE) when $E = 0$, where G_{AFE} and G_{PE} are the

free energy of AFE and PE state, and E_{tot} (AFE) and E_{tot} (PE) are the calculated total energy of AFE and PE structure by DFT, i.e. $\Delta G = G_{AFE} - G_{PE} = \Delta E = E_{AFE} - E_{PE}$ in Table S3. In Fig. S7a, the contour map of ΔG for $AgNbO_3$ is shown, in which four minima exist and are respectively marked as AFE and FE (ferrielectric). The AFE minima are for the nonpolar AFE phase with $P_A \neq 0$ and $P_F = 0$, while the ferrielectric minima correspond to the induced metastable polar ferrielectric phase with $P_A = 0$ and $P_F \neq 0$. Increasing E decreases ΔG_{Ferri}, while ΔG_{AFE} remains unchanged based on Equation (6). Hence, *E* induces the phase transition from AFE to ferrielectric in undoped $AgNbO_3$, as shown in Fig. S7d. For Nd-doped $AgNbO_3$ (Fig. S7b), the potential well becomes deeper [i.e. ΔG (Nd-doped $AgNbO_3$) < ΔG ($AgNbO_3$)], indicating that the AFE phase is more stable in Nd-doped than undoped $AgNbO_3$, in agreement with DFT results [i.e. ΔE_{tot} (Nd-doped $AgNbO_3$) < ΔE_{tot} ($AgNbO_3$) in Table S3]. In Fig. S7b, the AFE state ($P_A \neq 0$, $P_F = 0$) is more stable than the ferrielectric state ($P_A = 0$, $P_F \neq 0$) for Nd-doped $AgNbO_3$ when E = 0, but the converse is true when $E = E_F$ in Fig. S7e. Therefore, the induced electric field for AFE-ferrielectric phase transition (E_F) is larger for Nd-doped with respect to undoped $AgNbO_3$. We can conclude that Nd-doping leads to a more stable AFE structure, thereby increasing E_F (the onset of the AFE-ferrielectric induced phase transition in Fig. 4g). Similarly, for Nd/Ta co-doped $AgNbO_3$ in Fig. S7c, the potential well becomes much deeper [i.e. ΔG (Nd/Ta co-doped $AgNbO_3$) < ΔG (Nd-doped $AgNbO_3$) < ΔG ($AgNbO_3$)], indicating that the AFE phase is more stable in Nd/Ta co-doped than Nd-doped and undoped $AgNbO_3$, in agreement with DFT results [i.e. ΔE (Nd/Ta co-doped $AgNbO_3$) < ΔE_{tot} (Nd-doped $AgNbO_3$) < ΔE_{tot} ($AgNbO_3$) in Table S3]. In Fig. S7c, the AFE state ($P_A \neq 0$, $P_F = 0$) is much more stable than the ferrielectric state ($P_A = 0$, $P_F \neq 0$) for Nd/Ta co-doped $AgNbO_3$ when $E = 0$, but the converse is also true when $E = E_F$ in Fig. S7f.

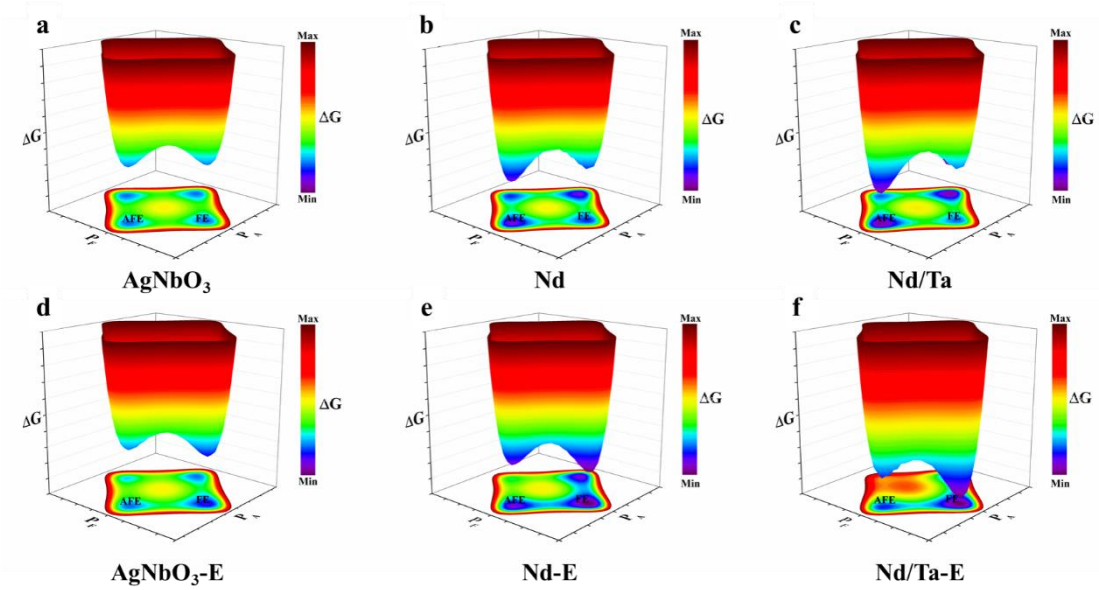

Fig. S7 Schematic contour diagrams of the free energy difference (ΔG) for (a) undoped $AgNbO_3$, (b) Nd-doped $AgNbO_3$, and (c) Nd/Ta co-doped $AgNbO_3$ systems without electric field. Schematic contour diagrams of LGD phenomenological theory of AFE-ferrielectric (FE) phase transition for (d) undoped $AgNbO_3$, (e) Nd-doped $AgNbO_3$, and (f) Nd/Ta co-doped $AgNbO_3$ with *E*.

Reference

1 P. Hohenberg, W. Kohn, Inhomogeneous electron gas, Phys. Rev. 136 (1964) B864-B871.

2 W. Kohn, L. J. Sham, Self-consistent equations including exchange and correlation effects, Phys. Rev. 140 (1965) A1133-A1138.

3 D. Vanderbilt, Soft self-consistent pseudopotentials in a generalized eigenvalue formalism, Phys. Rev. B 41 (1990) 7892-7895.

4 M. D. Segall, Philip. J. D. Lindan, M. J. Probert, C. J. Pickard, P. J. Hasnip, S. J. Clark, M. C. Payne, First-principles simulation ideas, illustrations and the CASTEP code, J. Phys. Condens. Matter 14 (2002) 2717-2744.

5 J. P. Perdew, A. Zunger, Self-interaction correction to density-functional approximations for many-electron systems. Phys. Rev. B 23 (1981) 5048-5079.

6 S. Liu, Y. Meng, S. Liu, D. Li, Y. Li, Y. Liu, Y. Shen, S. Wang, Compositional phase diagram and microscopic mechanism of $Ba_{1-x}Ca_xZr_yTi_{1-y}O_3$ relaxor ferroelectrics, Phys. Chem. Chem. Phys. 19 (2017) 22190-22196.

7 C. Kittel, Theory of antiferroelectric crystals, Phys. Rev. 82 (1951) 729-732.

8 P. Tolédano, M. Guennou, M. Theory of antiferroelectric phase transitions, Phys. Rev. B 94 (2016) 014107.